INTERNATIONAL JOURNAL FOR NUMERICAL METHODS IN FLUIDS
Int. J. Numer. Meth. Fluids 2008; **56**:383–400
Published online 6 June 2007 in Wiley InterScience (www.interscience.wiley.com). DOI: 10.1002/fld.1535

On the use of high-order finite-difference discretization for LES with double decomposition of the subgrid-scale stresses

J. Meyers[1,*,†], C. Lacor[2] and M. Baelmans[1]

[1]*Department of Mechanical Engineering, Katholieke Universiteit Leuven, Celestijnenlaan 300A, B3001 Leuven, Belgium*
[2]*Department of Fluid Mechanics, Vrije Universiteit Brussel, Pleinlaan 2, B1050 Brussel, Belgium*

SUMMARY

Large eddy simulation (LES) with additional filtering of the non-linear term, also coined LES with double decomposition of the subgrid-scale stress, is considered. In the literature, this approach is mainly encountered in combination with pseudo-spectral discretization methods. In this case, the additional filter is a sharp cut-off filter, which appears in the eventual computational algorithm as the 2/3-dealiasing procedure. In the present paper, the LES approach with additional filtering of the non-linear term is evaluated in a spatial, finite-difference discretization approach. The sharp cut-off filter used in pseudo-spectral methods is then replaced by a 'spectral-like' filter, which is formulated and discretized in physical space. As suggested in the literature, the filter width Δ of this spectral-like filter corresponds at least to $3/2$ times the grid spacing h to avoid aliasing. Furthermore, spectral-like discretization of the derivatives are constructed such that derivative-discretization errors are low in the wavenumber range resolved by the filter, i.e. $0 \leqslant kh \leqslant 2\pi/3$. The resulting method in combination with a Smagorinsky model is tested for decaying homogeneous isotropic turbulence and compared to standard lower-order discretization methods. Further, an analysis is elaborated of the Galilean-invariance problem, which arises when LES in double decomposition approach is combined with filters, which do not correspond to an orthogonal projection. The effects of a Galilean coordinate transformation on LES results, are identified in simulations, and we demonstrate that a Galilean transformation leads to wavenumber-dependent shifts of the energy spectra.

Received 15 September 2005; Revised 27 March 2007; Accepted 20 April 2007

KEY WORDS: LES; spectral-like discretization; Galilean invariance; homogeneous isotropic turbulence

*Correspondence to: J. Meyers, Department of Mechanical Engineering, Katholieke Universiteit Leuven, Celestijnenlaan 300A, B3001 Leuven, Belgium.
†E-mail: johan.meyers@mech.kuleuven.be

Contract/grant sponsor: FWO-Vlaanderen

1. INTRODUCTION

Large eddy simulation (LES) is evolving as an important simulation technique for the calculation of turbulent flows. The advantage of this technique is its relative low computational cost, compared to the direct simulation of the Navier–Stokes equations, while accurate results may still be obtained. In LES, this is achieved by filtering the original Navier–Stokes equations with a low-pass filter. The aim of this operation is to reduce the number of modes or length scales in the solution of the *filtered* Navier–Stokes equations, such that they can be solved on a much coarser grid, and hence, with a much lower cost, than direct numerical simulation would require.

The formal filtering of the Navier–Stokes equations is well established and described in several books and review articles, e.g. [1–5]. The crux of the matter, when filtering the Navier–Stokes equations, is the filtering of the non-linear term $u_i u_j$ (where u_i represents the ith component of the velocity field $\mathbf{u}$). In contrast to all other terms in the equations, the filtered non-linear term cannot be expressed directly in terms of filtered variables. To solve this, the non-linear term is typically split into a part which can be expressed as a function of filtered quantities and into a part which has to be closed with a model. Two main methodologies exist for this splitting [1, 6] i.e. following Leonard [7], and by introducing $u_i = \overline{u}_i + u_i'$, one obtains

$$\overline{u_i u_j} = \overline{\overline{u}_i \overline{u}_j} + \underbrace{\overline{\overline{u}_i u_j'} + \overline{u_i' \overline{u}_j}}_{C_{ij}} + \underbrace{\overline{u_i' u_j'}}_{R_{ij}} \tag{1}$$

The part which has to be closed, coined the subgrid-scale stresses, consists of two terms, i.e. the cross-stresses C_{ij} and the Reynolds stresses R_{ij}. Hence, the subgrid stresses τ_{ij} are

$$\tau_{ij} = \overline{\overline{u}_i \overline{u}_j} - \overline{u_i u_j} = -C_{ij} - R_{ij} \tag{2}$$

The corresponding filtered Navier–Stokes equation is

$$\frac{\partial \overline{u}_i}{\partial t} + \frac{\partial \overline{\overline{u}_i \overline{u}_j}}{\partial x_j} + \frac{\partial \overline{p}}{\partial x_i} - \frac{\partial \overline{\sigma}_{ij}}{\partial x_j} = \frac{\partial \tau_{ij}}{\partial x_j} \tag{3}$$

where σ_{ij} is the viscous stress term.

A second methodology for splitting the non-linear term corresponds to

$$\overline{u_i u_j} = \overline{u}_i \overline{u}_j + \underbrace{\overline{\overline{u}_i \overline{u}_j} - \overline{u}_i \overline{u}_j}_{L_{ij}} + \underbrace{\overline{\overline{u}_i u_j'} + \overline{u_i' \overline{u}_j}}_{C_{ij}} + \underbrace{\overline{u_i' u_j'}}_{R_{ij}} \tag{4}$$

with L_{ij} the Leonard stresses. The corresponding subgrid-stress tensor τ_{ij}^* is

$$\tau_{ij}^* = \overline{u}_i \overline{u}_j - \overline{u_i u_j} = -L_{ij} - C_{ij} - R_{ij} \tag{5}$$

These two approaches are labelled LES with double decomposition and LES with triple (or Leonard) decomposition, respectively, in Reference [1].

From a conceptual point of view, one might prefer the fact that LES with double decomposition retains only those terms in the subgrid-scale stresses, which cannot be expressed explicitly as a function of filtered quantities. This is in contrast to LES with triple decomposition, where L_{ij} can be expressed as a function of filtered quantities. However, the double decomposition approach

DOI: 10.1002/fld

also has conceptual disadvantages. In principle, Navier–Stokes equations are Galilean invariant. However, the non-linear term $\overline{\overline{u}_i \overline{u}_j}$, and therefore the subgrid-scale stresses τ_{ij} are not necessarily Galilean invariant [8], although their sum is. Both terms are Galilean invariant only, when $\overline{\overline{\mathbf{u}}} = \overline{\mathbf{u}}$. This occurs when the LES filter is an orthogonal projection filter such as, e.g. a spectral cut-off filter. As most subgrid-scale models are Galilean invariant, this introduces an extra difficulty. For non-orthogonal filters, the sum of a Galilean invariant subgrid-scale models and the non-linear term $\overline{\overline{u}_i \overline{u}_j}$ is not invariant under Galilean transformations. Consequently, for non-orthogonal filters, LES with double decomposition is not Galilean invariant.

On average, when LES filters are considered which do not correspond to an orthogonal projection filter, the triple decomposition approach is most often used. Without being complete, examples can be found in References [4, 9–14]. On the other hand, when orthogonal projection filters are available, i.e. most notoriously in pseudo-spectral methods, the double decomposition approach is common standard. In this case, the outer filter operation on the non-linear term $\overline{\overline{u}_i \overline{u}_j}$ corresponds often to the 2/3-dealiasing rule, e.g. References [15–21].

The aim of the present paper is to assess the implementation of LES with the double-decomposition approach in a finite-difference discretization context and to reduce corresponding discretization errors as much as possible. The advantage of finite-difference-discretization methods, or other discretization methods in physical space, such as finite volumes, is their flexibility in implementation and use, when complex geometries or additional complex physics such as combustion, multi-phase flow, etc. are involved. The advantage of the double-decomposition approach to LES is the unequivocal way in which errors can be identified into discretization errors on the one hand, including differencing and aliasing errors; and modelling errors on the other hand, e.g. [22]. Furthermore, discretization errors and modelling errors can be reduced independently from each other. In contrast, while using the triple-decomposition approach, errors are not as easily identified, and possible discretization and modelling errors can depend on each other in a complex way [10, 14].

In this paper, all presented LES results will refer to simulations with an additional filter on the non-linear term and two main challenges will be addressed with respect to the use of finite-difference discretization for LES in a double-decomposition approach, i.e.

1. The implementation of a spectral-like filter in physical space, using filter schemes first introduced in [23]. As proposed by Ghosal [22], the width Δ of the filter will be selected such that $\Delta \geqslant 3h/2$, with h the grid spacing of the discretization. This corresponds to the 2/3-dealiasing procedure [24] used in pseudo-spectral methods. Ghosal's proposal was tested before in Reference [25], where promising results were obtained with this methodology. The present paper provides supplementary results and in addition elaborates a careful evaluation of the Galilean-invariance issue, which appears when the outer filter on the non-linear term $\overline{\overline{u}_i \overline{u}_j}$ deviates from a sharp cut-off filter.
2. The formulation of differentiation schemes, which are spectral-like over a wide wavenumber range. Here compact schemes are used [23], which are tuned such that they provide an excellent accuracy in the wavenumber band $[0, \frac{2}{3}\pi/h]$. As such, they allow a minimal filter-width-to-grid-size ratio Δ/h, i.e. 3/2, when accounting for dealiasing.

The paper is further organized as follows. First, in Section 2, the filter and differentiation schemes in use are briefly discussed. Next, in Section 3, LES results are presented. Results obtained with

DOI: 10.1002/fld

standard discretization schemes of second and fourth order are compared to results of spectral-like discretization. Further, a comparison is presented between spectral-like and sharp cut-off filtering. Subsequently, the Galilean-invariance issue is elaborated in more detail in Section 4. Finally, conclusions are presented in Section 5.

2. DIFFERENTIATION AND FILTER SCHEMES

In the present section, a brief overview is presented of the schemes which are used to discretize the filter and differentiation operators. The specific schemes which are used, correspond with the general class of the compact schemes, on which a comprehensive discussion is presented in [23]. Throughout the discussion, the two main objectives presented at the end of Section 1, will be addressed.

First of all, for filtering, a class of central filters was proposed by Lele [23]:

$$\begin{aligned}&\beta\overline{\phi}_{i+2}+\alpha\overline{\phi}_{i+1}+\overline{\phi}_i+\alpha\overline{\phi}_{i-1}+\beta\overline{\phi}_{i-2}\\&\quad=a\phi_i+b\frac{\phi_{i+1}+\phi_{i-1}}{2}+c\frac{\phi_{i+2}+\phi_{i-2}}{2}+d\frac{\phi_{i+3}+\phi_{i-3}}{2}\end{aligned}\tag{6}$$

This scheme corresponds to a one-dimensional filter, which is successively applied in the three co-ordinate directions on the non-linear term. The filter kernel in Fourier space for this class of filters is given by

$$G(kh)=\frac{a+b\cos(kh)+c\cos(2kh)+d\cos(3kh)}{1+2\alpha\cos(kh)+2\beta\cos(2kh)}\tag{7}$$

$G(kh)$ is also coined the filter transfer function, where k is the wavenumber in Fourier space. For sake of non-dimensionalization, k is further multiplied in the argument of G with the grid spacing h.

In order to obtain values for the parameters α, β, a, etc. different constraints on $G(kh)$ can be set [23]. First of all, as a trivial requirement for a filter, $G(0)=1$ and $G(\pi)=0$ is required. Moreover, since $G(kh)$ is based on functions which are even at $kh=0$ and $kh=\pi$, all odd derivatives of $G(kh)$ evaluated at $kh=0$ or $kh=\pi$ are zero. Hence, extra possible constraints are

$$\begin{aligned}\left.\frac{\partial^2 G}{\partial k^2}\right|_{kh=0}&=0,\quad \left.\frac{\partial^4 G}{\partial k^4}\right|_{kh=0}=0,\quad\cdots\\\left.\frac{\partial^2 G}{\partial k^2}\right|_{kh=\pi}&=0,\quad \left.\frac{\partial^4 G}{\partial k^4}\right|_{kh=\pi}=0,\quad\cdots\end{aligned}\tag{8}$$

and further at certain values for kh, the value of G can be specified, e.g. $G(2\pi/3)=0.4$.

The sharpness which can be attained for a filter according to Equation (6) corresponds to the number of parameters selected different from zero. We take all parameters to be different from zero. Hence, apart from the two trivial constraints $G(0)=1$ and $G(\pi)=0$, four extra constraints are used. Monotonicity of the function $G(kh)$ in the interval $0\leqslant kh\leqslant\pi$ is achieved by selecting three constraints from Equation (8), and only one constraint remains which can be used to shift

DOI: 10.1002/fld

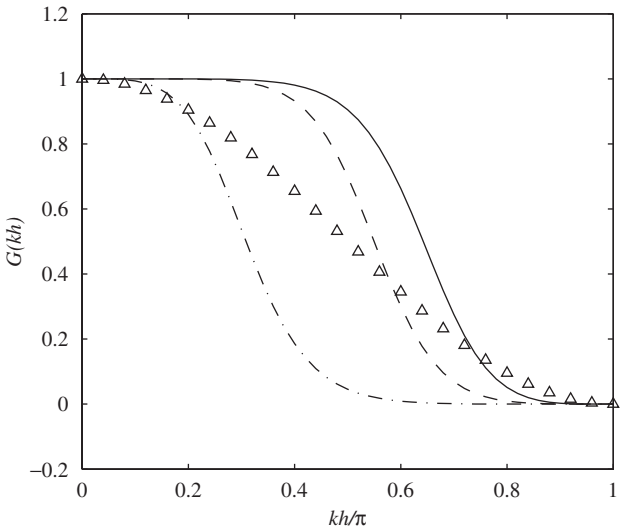

Figure 1. Transfer functions of different filters (cf. Table I). (△): top-hat filter ($\Delta = 2h$) approximated with trapezoid integration rule; (—): Filter A; (− −): Filter B; and (−·): Filter C.

the flank of $G(kh)$ to lower or higher values of k. This is illustrated in Figure 1, where three such monotonous filters are presented. The corresponding constraints and coefficients are listed in Table I. In addition, a top-hat filter (with trapezoid integration) is also displayed in Figure 1 and listed in Table I. The latter provides an impression of the relative 'sharpness' of the pentadiagonal filters compared to, e.g. top-hat or Gauss filters.

In the present paper, Filter A is used for the LES computations (cf. Section 3). As is observed in Figure 1, the point $G(kh) = 0.5$ is situated slightly to the left of $kh = 2\pi/3$, i.e. $G(2\pi/3) = 0.4$. We select this as an approximation of a sharp cut-off filter with width $\Delta = 3h/2$, i.e. corresponding to the minimum allowable filter width if aliasing is to be avoided (cf. Section 1). From Figure 1, it is obvious that a trade-off has to be made between an as-late-as-possible drop-off of $G(kh)$ in the region $kh < 2\pi/3$ on the one hand, and an as-fast-as-possible drop-off to zero in the region $kh > 2\pi/3$ on the other hand. In order to ensure better dealiasing behaviour, we slightly favour the latter desire by taking a pentadiagonal filter which is shifted a little to the left, i.e. $G(2\pi/3) = 0.4$ instead of 0.5. Naturally, other choices can be made. However, it is not in the scope of the present paper to present a full sensitivity analysis, but merely to show to potential of the methodology, and, as will be discussed in Section 3, the selected filter provides excellent results.

Next to filtering, the discretization of the differentiation operator is also performed with compact schemes [23], i.e.

$$\beta\phi'_{i+2} + \alpha\phi'_{i+1} + \phi'_i + \alpha\phi'_{i-1} + \beta\phi'_{i-2} = a\frac{\phi_{i+1} - \phi_{i-1}}{2h} + b\frac{\phi_{i+2} - \phi_{i-2}}{4h} + c\frac{\phi_{i+3} - \phi_{i-3}}{6h} \tag{9}$$

The transfer function of Equation (9) is

$$G(kh) = \frac{a\sin(kh) + (b/2)\sin(2kh) + (c/3)\sin(3kh)}{kh(1 + 2\alpha\cos(kh) + 2\beta\cos(kh))} \tag{10}$$

DOI: 10.1002/fld

Table I. Constraints and filter coefficients for various pentadiagonal filters.

Constraints	$\alpha, \beta, a, b, c, d$	Filter description
$G^{(2)}(0)=0$, $G^{(4)}(0)=0$, $G^{(2)}(\pi)=0$, $G(2\pi/3)=0.4$	$\alpha=0.479664$, $\beta=0.204067$, $a=0.859748$, $b=1.16971$, $c=0.323983$, $d=0.0140252$	Filter A
$G^{(2)}(0)=0$, $G^{(4)}(0)=0$, $G^{(2)}(\pi)=0$, $G(0.55\pi)=0.5$	$\alpha=0.190112$, $\beta=0.261978$, $a=0.642584$, $b=0.916348$, $c=0.309506$, $d=0.0357416$	Filter B
$G^{(2)}(0)=0$, $G^{(2)}(\pi)=0$, $G^{(4)}(\pi)=0$, $G(\pi/3)=0.4$	$\alpha=-0.57086$, $\beta=0.185828$, $a=0.0718553$, $b=0.107783$, $c=0.0431132$, $d=0.00718553$	Filter C
	$\alpha, \beta=0$, $a, b=\frac{1}{2}$, $c, d=0$	Top-hat filter ($\Delta=2h$) with trapezoid integration

Here G is defined using

$$G(kh)=\mathscr{F}\left\{\frac{D\phi}{Dx}\right\}\Big/\mathscr{F}\left\{\frac{\partial\phi}{\partial x}\right\} \tag{11}$$

where $\mathscr{F}\{\cdot\}$ is a Fourier transform. Further, D/Dx is a symbolic notation referring to the *discretized* derivative, while $\partial/\partial x$ refers to the exact derivation.

The different coefficients α, β, a, b and c can be selected based on several constraints. Lele [23] proposed to make a mix between high formal accuracy (i.e. order of the Taylor series truncation) on the one hand, and a good spectral behaviour of the transfer function over a wide wavenumber range on the other hand. The former is related to the behaviour of $G(kh)$ at $kh=0$; the latter can

DOI: 10.1002/fld

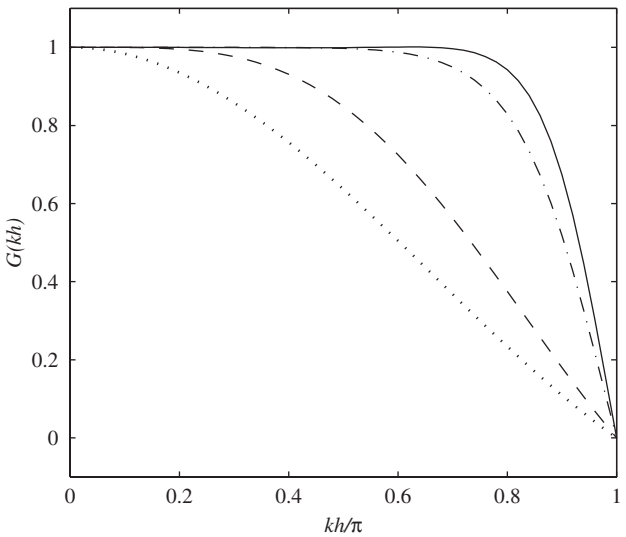

Figure 2. Derivative transfer functions *versus* wavenumber for various high-order and spectral-like central differencing schemes. (···): standard second-order scheme; (– –): standard fourth-order scheme; (–·): compact eighth-order scheme; and (—): spectral-like scheme. See also Table II.

Table II. Coefficients for various derivative-discretization schemes.

	β	α	a	b	c
Standard second order	0	0	1	0	0
Standard fourth order	0	0	4/3	−1/3	0
Compact eighth-order	0	3/8	25/16	1/5	−1/80
Spectral-like	0	0.421145	1.55849	0.317165	−0.0333647

be obtained by replacing formal accuracy constraints by constraints of the form $G(p) = 1$, where p is a carefully selected value for kh.

In Figure 2, several discretization schemes for the first derivative are compared. For reference, the coefficients of these schemes are listed in Table II. Next to standard second-order and fourth-order schemes, a compact eighth-order scheme is also presented. Further a four-parameter (α, a, b and c) spectral-like scheme is constructed of the same complexity as the eighth-order scheme, by requiring fourth-order formal accuracy and further $G(2\pi/3) = 1$ and $G(0.55\pi)$. This scheme is constructed to obtain good accuracy ($G \approx 1$) in the range $kh = 0$ to $2\pi/3$, which corresponds to the range of resolved scales associated with the minimum filter width $\Delta = 3h/2$ allowed for proper dealiasing. The specific choices $G(2\pi/3) = 1$ and $G(0.55\pi)$ are easily obtained from trial-and-error optimization, and various other combinations exist, which result in the same quality.

The combination of a sharp cut-off filter or spectral-like cut-off filter, with cut-off $k_c h = 2\pi/3$, and a spectral-like discretization scheme which is accurate over the wavenumber range $0 \leqslant kh \leqslant 2\pi/3$, is optimal with respect to the computational resources which are needed to resolve LES with

DOI: 10.1002/fld

Table III. Total number of floating point operations used for different discretization schemes which are, using appropriate grid refinement, roughly at the same accuracy (assignments are not counted).

	$\partial/\partial x_1$	Filtering (1D)
Second order	$512(\mathscr{L}/\Delta)^4$	$5888(\mathscr{L}/\Delta)^4 - 1088(\mathscr{L}/\Delta)^3$
Fourth order	$80(\mathscr{L}/\Delta)^4$	$368(\mathscr{L}/\Delta)^4 - 272(\mathscr{L}/\Delta)^3$
Spectral-like	$\frac{513}{8}(\mathscr{L}/\Delta)^4 - \frac{9}{4}(\mathscr{L}/\Delta)^3$	$\frac{1863}{16}(\mathscr{L}/\Delta)^4 - \frac{459}{8}(\mathscr{L}/\Delta)^3$

Table IV. Number of floating point operations (assignments are not counted) for matrix inversion of compact schemes (cf. Reference [26] for a detailed overview).

	Non-periodic boundary conditions	Periodic boundary conditions
$\alpha \neq 0, \beta \neq 0$	$9n - 12$	$13n - 17$
$\alpha \neq 0, \beta = 0$	$5n - 4$	$7n - 2$
$\alpha = 0, \beta \neq 0$	$5n - 4$	$7n - 2$ (n even) $9n - 12$ (n odd)

a filter width Δ. Indeed, consider LES with double decomposition using a sharp cut-off filter with filter width Δ and corresponding cut-off wavenumber $k_c = \pi/\Delta$. To accurately discretize the corresponding filtered Navier–Stokes equations (Equation (3)), a grid of spacing h is used. To avoid dealiasing, the ratio Δ/h should be at least $3/2$. However, depending on the choice of discretization scheme, this required ratio can be much higher for accuracy reasons. For standard second-order central schemes, a rather optimal estimation might be $\Delta/h = 4$, while for standard fourth-order schemes, at least a ratio $\Delta/h = 2$ might be in order. Hence for the same choice of Δ, a second-order scheme requires the finest grid. The corresponding differences in computational time can be large. For instance, for a standard second-order scheme, the number of cells n in one direction corresponds to $n = 4\mathscr{L}/\Delta$ (assuming $\Delta/h = 4$ is required, and taking $\mathscr{L}$ the size of the computational domain). The number of time steps needed to integrate the equations over a period T, is—by means of a CFL-criterion—proportional to n. Hence, the total number of operations (ignoring assignments, counting only $+$, $-$, $\times$ and $/$) to spend on the calculations of, e.g. $\partial/\partial x_1$ is easily estimated as being proportional to $2(4\mathscr{L}/\Delta)^4 = 512(\mathscr{L}/\Delta)^4$. Similarly, for a standard fourth-order scheme ($n = 2\mathscr{L}/\Delta$) and for the spectral-like scheme presented in Table II ($n = \frac{3}{2}\mathscr{L}/\Delta$), an operation count can be performed. An overview is presented in Table III. The operation count for the spectral-like scheme is partially supported by the detailed operation count of the matrix-inversion algorithms, which are briefly summarized in Table IV. An extensive overview of the matrix-inversion algorithms and their operation count can be found in Reference [26].

Comparison of the three schemes in Table III shows that the discretization of $\partial/\partial x_1$ using a fourth-order scheme is up to six times faster than the second-order scheme, while the use of a spectral-like scheme is up to eight times faster than the use of a second-order scheme. When comparing the number of operations spent on a one-dimensional spectral-like filter operation (with a pentadiagonal filter and all coefficients $\neq 0$), the difference is even more pronounced. In this

DOI: 10.1002/fld

case, the fourth-order discretization is 16 times faster than the second-order discretization, while the spectral-like discretization is up to 50 times faster. This analysis clearly illustrates the advantage of discretization schemes which allow, with respect to accuracy, for a filter-to-grid ratio Δ/h close to $3/2$.

The discretization of second derivatives can be based on the same principles as that of the first derivative. The discretization of cross-derivatives $\partial/\partial x_i \partial x_j, i \neq j$ is a straightforward combination of two first-derivative schemes in different spatial directions. For the discretization of $\partial^2/\partial x_i^2$ two approaches are compared. First of all a tridiagonal spectral-like scheme for the discretization of the second derivative is constructed [23] and used. Secondly, the second derivative is constructed by a subsequent operation of two first derivatives in the same direction. The latter is in general considered bad practice, since it typically causes decoupling of the equations and results in instabilities. However, for the spectral-like compact scheme used here, both approaches give identical results. When, e.g. standard fourth-order schemes are used, this is not anymore the case, and instabilities are observed indeed for the second approach. Actual LES results will be presented in the next section, with main emphasis on the first-derivative discretization, while the second-derivative discretization is always implemented conform to the scheme used for the first derivative.

We discussed the construction of compact spectral-like schemes in finite-difference discretization. The implementation of compact schemes can be extended to finite-volume methods on arbitrary meshes, such that the presented methodology is also applicable for finite-volume codes and more complex applications. More details on the implementation of compact schemes in a finite-volume context can, e.g. be found in [27, 28].

3. APPLICATION OF SPECTRAL-LIKE DISCRETIZATION IN LES

We apply the techniques introduced in the previous section on decaying homogeneous isotropic turbulence. This allows for the methodical evaluation of two different effects. First of all, the effectiveness of the pentadiagonal filtering of the non-linear term is evaluated and compared with sharp cut-off dealiasing. Secondly, the quality of simulations using spectral-like discretization and filtering is compared to the results which are obtained with standard second- and fourth-order approaches to LES discretization. All results are further compared to DNS reference data.

Before turning to the evaluation of these two effects, we first briefly introduce some further details on the test case, and the numerical set-up of the simulations. The reference DNS is performed on a 256^3 box with size $\mathscr{L} = 2\pi$, which was run using a dealiased pseudo-spectral code [29]. The LES is started by truncating the DNS solution at $t_{\mathrm{DNS}} \approx 4.17$ (for the LES run, $t = 0$ at this point) and using this field as an initial condition. The initial Taylor Reynolds number $Re_\lambda \approx 90$. Further, the Kolmogorov scale approximately corresponds to $\mathscr{L}/400$.

LESs are performed on a 36^3 grid. To generate the initial condition, the DNS is truncated in spectral space to 24 modes, and padded with zeros up to 36 modes, hence allowing a $\frac{2}{3}$-dealiasing procedure in physical space as described in the previous section. The LES is performed with the EURANUS solver,[‡] which is a compressible Navier–Stokes solver. The different compact

[‡]The EURANUS solver was originally developed at VUB (Brussels, Belgium) and FFA (Sweden) in the framework of the ESA/ESTEC contract 8356/98/NL/FG. At present, this solver is part of the FINE/TURBO package, which is developed and distributed by Numeca International. This company originated as a spin-off of the Department of Fluid Mechanics, Vrije Universiteit Brussel.

DOI: 10.1002/fld

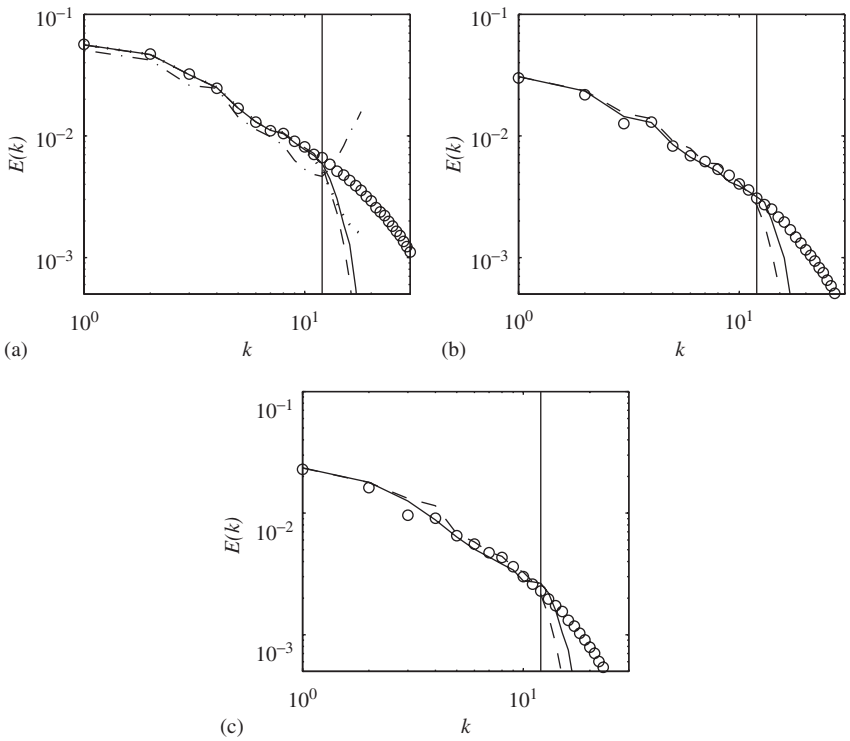

Figure 3. DNS reference [29] and LES spectra at three time instances. (○): DNS; (—): case 1, LES with sharp cut-off dealiasing; (− −): case 2, LES with compact pentadiagonal dealiasing; (· · ·): case 3, LES without dealiasing (only in (a)); (–·): case 1 at point of divergence (occurs at $t \approx 0.73$, therefore presented in (a)); (a) $t \approx 0.33$. (b) $t \approx 3.33$. (c) $t \approx 4.83$.

formulations are implemented in this solver. For the time integration, a second-order five-stage low-storage Runge–Kutta scheme is used. The time stepping is limited with a CFL number of 2. The computations are run at a Mach number $M = 0.2$, such that compressibility effects are negligible.

The effectiveness of pentadiagonal filtering of the non-linear term is now elaborated. To this end, three different cases are compared, all of them using a spectral-like compact scheme for the discretization (cf. Figure 2, spectral-like A). First (case 1), as a reference case, dealiasing is performed using a cubical sharp cut-off filter which is implemented using forward and backward Fourier transforms. In a second case (2), the filtering of the non-linear term is performed based on a pentadiagonal filter in physical space. This filter corresponds to Filter A in Table I. Finally, a case is run (case 3) without the use of dealiasing or filtering of the non-linear term. For all three cases, we use a constant-coefficient Smagorinksy model with $C_s = 0.16$, which is a common accepted value for homogeneous turbulence. We do not use a dynamic procedure, since we want to avoid that differences between the cases are concealed by a different dynamic selection of Smagorinsky constants.

In Figure 3, three-dimensional energy spectra are presented for these three cases and compared to DNS data at three different time instances in the simulation, i.e. $t = 0.33$, $t = 3.33$ and $t = 4.83$.

DOI: 10.1002/fld

In all plots, the filter cut-off wavenumber (at $k = \frac{2}{3}\pi/h$) is also displayed. Beyond this wavenumber, energy spectra still show a small amount of energy. For these wavenumbers $k > \frac{2}{3}\pi/h$, wavenumber spheres in three-dimensional Fourier space only partially intersect with the cubical computational box. Hence, integration over wavenumber spheres to obtain the energy spectrum is not complete for these values of k. We elected to display these 'partial' modes since they more clearly highlight possible high-wavenumber energy pile up and divergence. Evidently, in this range, the comparison between LES and DNS is irrelevant.

First of all, case 3 (Figure 3) is not stable and diverges shortly after $t \approx 0.8$. The divergence of case 3 is clearly induced by an increase of the energy in the smallest scales. This event does not result from any physical turbulence phenomenon, but is solely related to the dealiasing error. Both cases 1 and 2, where some form of dealiasing is used, provide reasonable results as can be seen in Figure 3(a)–(c). Further, the use of pentadiagonal filters provides a slightly higher energy during the calculation than seen in the sharp-cut-off-dealiasing case. However, these differences are minimal.

We now turn to the comparison of spectral-like discretization of the derivatives to a fourth-order discretization method, both using sharp-cut off dealiasing. Next to this, results from a standard second-order method without dealiasing are also included. The last case can be considered as a 'low-quality' reference. In contrast to the simulations discussed in Figure 3, we now use a dynamic Smagorinsky model [30]. In this way, every method is allowed to obtain its optimal model coefficient [31, 32] without partiality in the selection of C_s.

In Figure 4 results are presented. We emphasize that the spectral-like and fourth-order cases use only 24 of the possible 36 modes available on a 36^3 grid, since the last third of the modes is removed with a sharp cut-off filter to avoid aliasing. The second-order case does not use dealiasing and utilizes the full 36 modes. However, as can be appreciated in Figure 4(b) and (c), the second-order results are clearly inferior to both higher-order methods in spite of their decrease in effective resolution. In fact, the standard second-order LES implementation induces too much dissipation of energy in the large turbulent scales, while at the same time, too much energy is found at the tail of the spectrum (note that this simulation does not diverge). This type of pile up may in part result from too low values for the Smagorinsky coefficient [33]. Further, the absence of dealiasing typically leads to a spurious injection of extra energy in the high-wavenumber range of the spectrum (see e.g. [24]). An overestimation of the smallest-scale kinetic energy then results in a too high kinetic-energy transfer rate from large to small scales due to triadic interactions, i.e. an accelerated forward energy cascade process, leading to an underestimation of the large-scale energy.

When both high-order methods are compared in Figure 4, the spectral-like scheme clearly prevails compared to the fourth-order method. The fourth-order method displays too much dissipation at low wavenumbers ($4 \leqslant k \leqslant 7$) and a slight energy pile-up at large wavenumbers. The effects are however relatively small compared to the deficiencies in the second-order LES.

The results in the present section allow us to draw three main conclusions. First of all, spectral-like discretization schemes can only be used in combination with dealiasing. In case the dealiasing is omitted, the simulations diverge at coarse resolution. Second, the replacement of a sharp cut-off filter with a pentadiagonal filter does not significantly influence the results, indicating that the latter is a good approximation to a sharp cut-off filter for dealiasing purposes. Third, a comparison of spectral-like schemes with dealiasing, with a standard second-order finite-volume method, clearly indicates superior results for the spectral-like schemes, even though the effective resolution for

DOI: 10.1002/fld

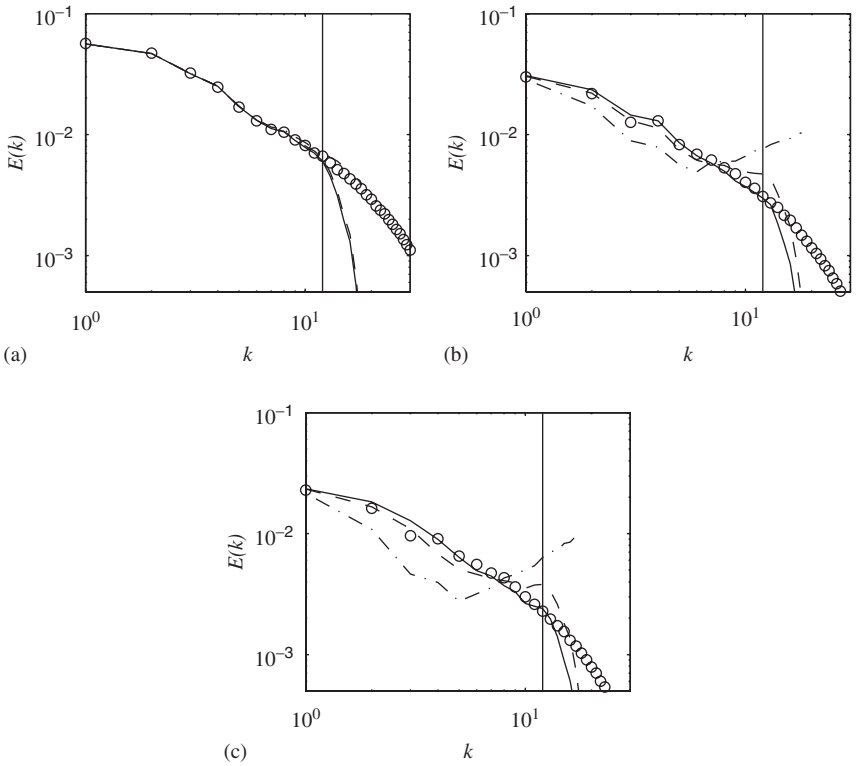

Figure 4. DNS reference [29] and LES spectra for different discretization methods. (◯): DNS; (—): LES with sharp cut-off dealiasing and spectral-like discretization; (− −): LES with sharp cut-off dealiasing and fourth-order discretization; (–·): standard second-order LES without dealiasing; (a) $t \approx 0.33$. (b) $t \approx 3.33$. (c) $t \approx 4.83$.

these schemes corresponds only to $2/3$ of the resolution available to the standard second-order method.

A further elaboration on the approximation of a sharp cut-off filter with a pentadiagonal filter is presented in the next section, addressing the Galilean-invariance issue.

4. GALILEAN INVARIANCE

The problem of Galilean invariance and LES with double decomposition has already been introduced (cf. Section 1). Here, this issue, introduced by [8], is briefly reviewed and further elaborated. The lack of Galilean invariance of the filtered Navier–Stokes equations in the double-decomposition formulation, when pentadiagonal sharp cut-off like filters are used, is evaluated theoretically as well as numerically.

Consider the coordinate frame x_i^b, which is a Galilean transformation of reference coordinate frame x_i^a:

$$x_i^b = x_i^a + \mathscr{U}_i t \tag{12}$$

DOI: 10.1002/fld

with $\mathscr{U}_i$ the relative velocity between both coordinate frames. Hence,

$$u_i^b = u_i^a + \mathscr{U}_i \tag{13}$$

and further

$$\langle u_i^b \rangle = \langle u_i^a \rangle + \mathscr{U}_i \tag{14}$$

$$\overline{u}_i^b = \overline{u}_i^a + \mathscr{U}_i \tag{15}$$

$$u_i'^b = u_i'^a \tag{16}$$

With the use of Equation (15), it is possible to express a relation between τ_{ij}^b and τ_{ij}^a. In fact,

$$\begin{aligned}\tau_{ij}^b &= \overline{\overline{u}_i^b \overline{u}_j^b} - \overline{u_i^b u_j^b} \\ &= \overline{(\overline{u}_i^a + \mathscr{U}_i)(\overline{u}_j^a + \mathscr{U}_j)} - \overline{(u_i^a + \mathscr{U}_i)(u_j^a + \mathscr{U}_j)}\end{aligned} \tag{17}$$

and hence, it follows straightforwardly that

$$\tau_{ij}^b = \tau_{ij}^a + \mathscr{U}_i(\overline{\overline{u}}_j^a - \overline{u}_j^a) + (\overline{\overline{u}}_i^a - \overline{u}_i^a)\mathscr{U}_j \tag{18}$$

similarly, for the cross and Reynolds stresses (cf. Equation (2)), one obtains

$$C_{ij}^b = C_{ij}^a + \mathscr{U}_i(\overline{\overline{u}}_j^a - \overline{u}_j^a) + (\overline{\overline{u}}_i^a - \overline{u}_i^a)\mathscr{U}_j \tag{19}$$

and

$$R_{ij}^b = R_{ij}^a \tag{20}$$

Equation (18) clearly illustrates that τ_{ij} is not Galilean invariant, but depends on the reference frame it is expressed in. This can be totally attributed to the fact that the cross-terms C_{ij} are not Galilean invariant, as demonstrated in Equation (19), while the Reynolds stresses are Galilean invariant.

From Equation (18), it is straightforward to define the difference between the subgrid terms cast in different reference frames:

$$\delta_{\mathrm{sgs},ij}^{ab} = \tau_{ij}^a - \tau_{ij}^b = \mathscr{U}_i(\overline{u}_j^a - \overline{\overline{u}}_j^a) + (\overline{u}_i^a - \overline{\overline{u}}_i^a)\mathscr{U}_j \tag{21}$$

Following the same procedure, one can readily derive that the difference between non-linear terms, cast in different reference frames, results into the same relation, i.e.

$$\delta_{nl,ij}^{ab} = \delta_{\mathrm{sgs},ij}^{ab} \tag{22}$$

Since both differences occur at the left-hand side and right-hand side of the filtered Navier–Stokes equations, respectively, it is evident that the full equations remain Galilean invariant. However, when the subgrid-scale stress is replaced with a Galilean invariant model, $\delta_{nl,ij}^{ab}$ in the left-hand side of the closed-LES equations will not be balanced by a term on the right-hand side. Hence, in this case, the closed-LES equations are not Galilean invariant.

DOI: 10.1002/fld

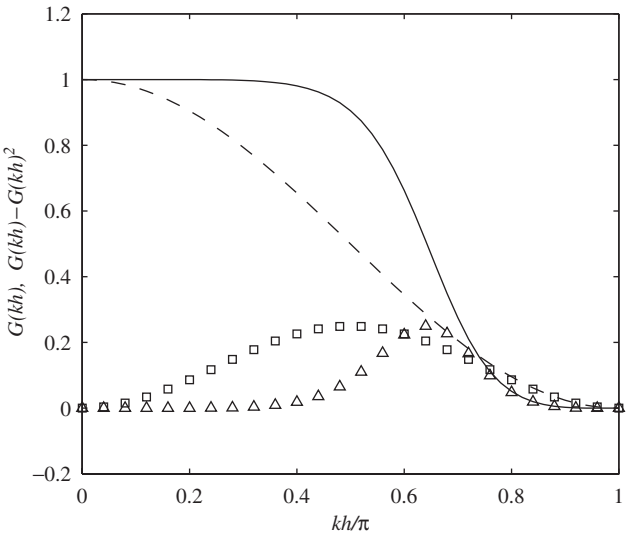

Figure 5. $G(kh)$ and $G(kh) - (G(kh))^2$ for the top-hat filter approximated with a trapezoidal integration rule and for pentadiagonal Filter A (cf. Table I). (—): pentadiagonal Filter A; (△): $G(kh) - (G(kh))^2$ corresponding to pentadiagonal Filter A; (– –): top-hat filter approximation; (□): $G(kh) - (G(kh))^2$ corresponding to top-hat filter approximation.

The effective difference in the subgrid force between coordinate frame $\mathbf{x}^a$ and $\mathbf{x}^b$ corresponds to $\partial \delta^{ab}_{\text{sgs},ij}/\partial x_j$ (summation over repeated j index). Its Fourier transform yields

$$\mathscr{F}\left\{\frac{\partial \delta^{ab}_{\text{sgs},ij}}{\partial x_j}\right\} = [G(\mathbf{k}) - (G(\mathbf{k}))^2](\mathscr{U}_i I k_j u_j(\mathbf{k}) + I k_j u_i(\mathbf{k}) \mathscr{U}_j) \tag{23}$$

with I the imaginary unit. By using $k_j u_j = 0$, i.e. expressing continuity in Fourier space for incompressible flows this further reduces to

$$\mathscr{F}\left\{\frac{\partial \delta^{ab}_{\text{sgs},ij}}{\partial x_j}\right\} = [G(\mathbf{k}) - (G(\mathbf{k}))^2] I k_j u_i(\mathbf{k}) \mathscr{U}_j \tag{24}$$

Clearly, when $G(\mathbf{k})$ corresponds to a sharp cut-off filter, $\delta^{ab}_{\text{sgs},ij} = 0$, since $G(\mathbf{k}) - (G(\mathbf{k}))^2 = 0$ in this case. However, when $G(\mathbf{k})$ deviates from a sharp cut-off filter, as is the case with the pentadiagonal filters in Section 2, a difference is present. The effective difference in subgrid force then depends on the scales present in $\mathbf{u}(\mathbf{k})$. When the subgrid-scale model is Galilean invariant, it is exactly this frame-of-reference-dependent force, which will distort the solution.

In Figure 5, $G(kh) - (G(kh))^2$ is presented for two different filters: on the one hand, the trapezoidal approximation of the top-hat filter, and, on the other hand, the pentadiagonal Filter A (cf. Table I). From this, it follows that $\partial \delta^{ab}_{\text{sgs},ij}/\partial x_j$ has an influence on a broad range of scales. This is distinctly the case for the top-hat approximation, where all wavenumbers are influenced. In contrast, for the pentadiagonal filter, the influence is mainly concentrated around the filter cut-off, i.e. for $0.5 < kh < 0.8$.

DOI: 10.1002/fld

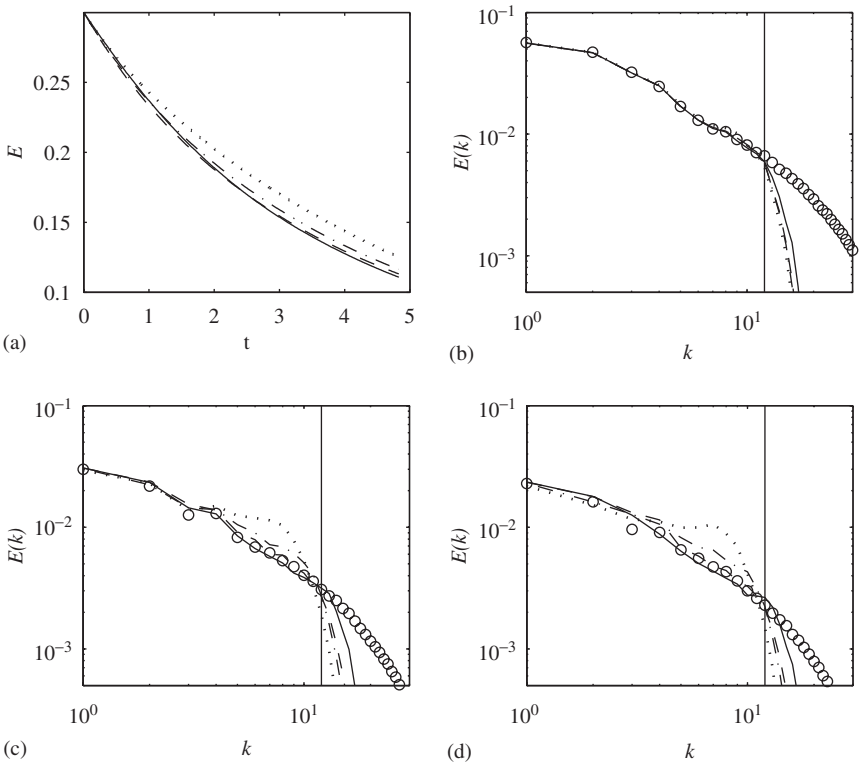

Figure 6. Influence of a Galilean shift of reference frame on LES with a constant Smagorinsky model. (◯): DNS reference [29] (—): LES with sharp cut-off dealiasing; (– –): LES with pentadiagonal dealiasing; (–·): LES with pentadiagonal dealiasing and Galilean shift of reference frame with $\mathscr{U}_i = 1$; (· · ·): LES with pentadiagonal dealiasing and Galilean shift of reference frame with $\mathscr{U}_i = 6$; (a) Decay of kinetic energy. (b) Energy spectrum at $t \approx 0.33$. (c) Energy spectrum at $t \approx 3.33$. (d) Energy spectrum at $t \approx 4.83$.

In order to check the relevance of Galilean invariance in actual simulations, LES with a Smagorinsky model, with and without a Galilean shift of reference frame is performed. Reference is an LES, where the dealiasing is performed using a sharp cut-off filter. Further, three different LES with pentadiagonal dealiasing are performed, corresponding to a stationary coordinate frame, a coordinate frame with velocity shift $\mathscr{U}_i = 1$ and one with $\mathscr{U}_i = 6$, respectively. In addition, to exclude time integration effects (due to the velocity shift, the magnitude of the maximum absolute velocity and hence the time step differs), LES with sharp cut-off dealiasing is also performed in the shifted reference frames. As might be expected, in case of sharp cut-off dealiasing, results in all reference frames are exactly the same. In Figure 6, sharp cut-off dealiased LES is compared to the cases where pentadiagonal dealiasing is used.

First of all, from Figure 6(a), it is clear that the influence on the energy decay is already relevant for a relatively small velocity shift $\mathscr{U}_i = 1$. Here, the relative magnitude of the velocity shift can be appreciated inversely proportional to $u/\mathscr{U}_i$, with $u = (u_i u_i/3)^{1/2}$ the rms-velocity fluctuation. This corresponds to the turbulence intensity of a flow with mean velocity $\mathscr{U}_i$, which transports the homogeneous isotropic turbulence. In case $\mathscr{U}_i$ equals one, $u/\mathscr{U}_i \approx 25\%$. Typically, e.g. in

DOI: 10.1002/fld

channel flows, mixing layers, the turbulence intensities can be considerably lower, thus inducing a relatively higher velocity shift if the reference frame is transformed from a stationary one to a reference frame which moves with the mean flow velocity. For example, the well-known Comte–Bellot experiment on grid turbulence [34] is performed in a wind tunnel with a turbulence intensity $u/\mathscr{U}_i \approx 2\%$. For $\mathscr{U}_i = 6$, in the present computation, the turbulence intensity $u/\mathscr{U}_i \approx 5\%$. For this case, the results in Figure 6 differ considerably from those in the original reference frame.

In Figure 6(b)–(d), the corresponding spectra at three different times are shown. Again, the influence of the shift of reference frame, certainly for the $\mathscr{U}_i = 6$ case, can be appreciated. Moreover, the wavenumber dependence of the difference, as is suggested by Equation (24) and Figure 5, can be readily observed and is mainly situated in the intermediate to high-wavenumber range.

To conclude, the Galilean invariance property of the LES equations in double-decomposition formulations are not satisfied when sharp cut-off-like pentadiagonal filters and Galilean invariant models are used. The resulting differences in simulation when a Galilean transformation is applied can be quite substantial. To counter this, one can add a correction term which is not Galilean invariant to a Galilean invariant model m_{ij}, i.e. by taking

$$\tau_{ij} \rightarrow m_{ij} + \mathscr{U}_i(\overline{\overline{u}}_j - \overline{u}_j) + (\overline{\overline{u}}_i - \overline{u}_i)\mathscr{U}_j \tag{25}$$

It is readily seen that a Galilean shift of reference frame with a velocity $\mathscr{U}_i$ now results in exactly the same solution. However, from a model point of view, Equation (25) introduces a new ambiguity. Indeed, $\mathscr{U}_i$ represents the *relative* velocity difference between two reference frames. However, there does not exist a unique standard reference frame, which allows to define $\mathscr{U}_i$ in *absolute* sense. Consequently, observations on subgrid-scale models and results cannot straightforwardly be generalized. This is a drawback, which should be carefully taken into account, when LES with double decomposition spectral-cut-off-like filtering is used.

5. CONCLUSIONS

The use of spectral-like finite-difference schemes for the discretization of the filtered Navier–Stokes equations with additional filter on the non-linear term has been investigated. The additional filter on the non-linear term corresponds with a double decomposition of the subgrid-scale stresses. This approach to the formulation of the LES equations is mainly encountered in the context of pseudo-spectral discretization. In the present paper, the potential of this approach for finite-difference-discretization methods is elaborated. Emphasis was on the accurate formulation of the derivative discretization on the one hand, and further, on the spatial formulation of a 'sharp' in the sense of steep filter, which can be used as a replacement of a sharp cut-off filter.

First of all, spectral-like filters are constructed with use of compact schemes [23]. Pentadiagonal filters, with six parameters are used. These parameters are selected such that the filter is monotonous in the interval $0 \leqslant kh \leqslant \pi$, and has a cut-off situated approximately at $kh = 2\pi/3$. This ensures that aliasing errors are minimal. Actual LES, using this filter on the non-linear term are performed, and compared with LES where a sharp cut-off filter is used. Results are satisfactory when compared with DNS, and differences between the pentadiagonal filtered LES and the sharp cut-off filtered LES are small.

Second, the use of spectral-like compact schemes [23] for the discretization of derivatives is assessed. The coefficients of the scheme are determined such that discretization errors are low in the wavenumber range $0 \leqslant kh \leqslant 2\pi/3$, which, for dealiasing reasons, corresponds to the maximum

DOI: 10.1002/fld

resolved wavenumber range. LES results using these schemes combined with filtering of the non-linear term provides good results, which are significantly better than a standard second-order method without additional filtering. When results for spectral-like schemes are compared with LES using fourth-order discretization, spectral-like discretization again provides better results, but differences are less pronounced.

LES with double decomposition of the subgrid term, which corresponds to an additional filter operation on the non-linear term, does only provide a Galilean invariant non-linear term when this filter is a sharp cut-off filter. In case a spectral-like filter is used, combined with a Galilean invariant model, such as the Smagorinsky model, this causes a set of LES equations which are not invariant under Galilean transformations. The corresponding deviation of the results, when a Galilean transformation is performed, is shown to be wavenumber dependent, i.e. mainly occurs in the mid- to high-wavenumber range. Actual numerical results in different reference frames, show considerable differences, which cannot be neglected. This observation certainly is a drawback for the formulation of LES with double decomposition in a finite-difference discretization context, and should be carefully taken into account when this approach is used.

The current work has concentrated on simulations of decaying homogeneous isotropic turbulence. Obviously, the presented numerical schemes have to be checked in different simulation environments, such as channel flows, jets or mixing layers, and next to DNS, comparison with higher Reynolds number experimental data is appropriate. In this context, some results and generalizations can be found in References [27, 28, 35]. However, the type of detailed error analysis which can be performed in homogeneous isotropic turbulence, makes this a unique case for the testing of basic discretization principles. The quantification of the Galilean invariance issue in current paper is a clear demonstration of this. Detailed error analysis in more complex cases, including Galilean-invariance effects on the solutions, is subject of ongoing research.

ACKNOWLEDGEMENTS

This research was performed in the framework of FWO-project G.0130.02. The authors would like to express their gratitude for the financial support by FWO-Vlaanderen.

REFERENCES

1. Sagaut P. *Large Eddy Simulations for Incompressible Flows* (2nd edn). Scientific Computation. Springer: Berlin, 2002.
2. Geurts BJ. *Elements of Direct and Large-edddy Simulation*. RT Edwards Inc: Flourtown, 2003.
3. Lesieur M, Métais O. New trends in large-eddy simulations of turbulence. *Annual Review in Fluid Mechanics* 1996; **28**:45–82.
4. Mason PJ. Large-eddy simulation: a critical review of the technique. *Quarterly Journal of the Royal Meteorological Society* 1994; **120**:1–26.
5. Rogallo RS, Moin P. Numerical simulations of turbulent flows. *Annual Review in Fluid Mechanics* 1984; **16**:99–137.
6. Winckelmans GS, Lund TS, Carati D, Wray AA. A priori testing of subgrid-scale models for the velocity–pressure and vorticity–velocity formulations. *Center for Turbulence Research Proceedings of the Summer Program*, Stanford, U.S.A., 1996.
7. Leonard A. Energy cascade in large-eddy simulations of turbulent fluid flows. *Advances in Geophysics* 1974; **18**:237–248.
8. Speziale CG. Galilean invariance of subgrid-scale stress models in the large-eddy simulation of turbulence. *Journal of Fluid Mechanics* 1985; **156**:55–62.

DOI: 10.1002/fld

9. Vreman B. Direct and large-eddy simulation of the compressible turbulent mixing layer. *Ph.D. Thesis*, Department of Applied Mathematics, University of Twente, 1995.
10. Vreman B, Geurts B, Kuerten H. Comparison of numerical schemes in large-eddy simulations of the temporal mixing layer. *International Journal for Numerical Methods in Fluids* 1996; **22**:297–311.
11. Mason PJ, Brown AR. On subgrid models and filter operations in large eddy simulations. *Journal of the Atmoshperic Sciences* 1999; **56**:2101–2114.
12. Magnient J-C, Sagaut P, Deville M. A study of built-in filter for some eddy viscosity models in large-eddy simulation. *Physics of Fluids* 2001; **13**(5):1440–1449.
13. Geurts BJ, Fröhlich J. A framework for predicting accuracy limitations in large eddy simulations. *Physics of Fluids* 2002; **14**(6):L41–L44.
14. Meyers J, Geurts BJ, Baelmans M. Database-analysis of errors in large-eddy simulation. *Physics of Fluids* 2003; **15**(9):2740–2755.
15. Métais O, Lesieur M. Spectral large-eddy simulation of isotropic and stably stratified turbulence. *Journal of Fluid Mechanics* 1992; **293**:157–194.
16. Ghosal S, Lund TS, Moin P, Akselvoll KA. A dynamic localization model for large-eddy simulation of turbulent flows. *Journal of Fluid Mechanics* 1995; **286**:229–255.
17. Spyropoulos ET, Blaisdell GA. Evaluation of the dynamic subgrid-scale model for large eddy simulations of compressible turbulent flows. *Technical Report 95-0355*, AIAA, 1995.
18. Meneveau C, Lund TS, Cabot WH. A lagrangian dynamic subgrid-scale model of turbulence. *Journal of Fluid Mechanics* 1996; **319**:353–385.
19. Domaradzki JA, Saki EM. A subgrid-scale model based on the estimation of unresolved scales of turbulence. *Physics of Fluids* 1997; **9**(7):2148–2165.
20. Dantinne G, Jeanmart H, Winckelmans GS, Legat V. Hyperviscosity and vorticity-based models for subgrid scale and modeling. *Applied Scientific Research* 1998; **59**:409–420.
21. Carati D, Rogers MM, Wray AA. Statistical ensemble of large-eddy simulations. *Journal of Fluid Mechanics* 2002; **455**:195–212.
22. Ghosal S. An analysis of numerical errors in large-eddy simulations of turbulence. *Journal of Computational Physics* 1996; **125**:187–206.
23. Lele SK. Compact finite difference schemes with spectral-like resolution. *Journal of Computational Physics* 1992; **103**:16–42.
24. Canuto C, Hussaini MY, Quarteroni A, Zang TA. *Spectral Methods in Fluid Dynamics*. Springer Series in Computational Physics. Springer: Berlin, 1988.
25. Fedioun I, Lardjane N, Gökalp I. Revisiting numerical errors in direct and large eddy simulations of turbulence: physical and spectral analysis. *Journal of Computational Physics* 2001; **174**:816–851.
26. Meyers J. Accuracy of large-eddy simulation strategies. *Ph.D. Dissertation*, Department of Mechanical Engineering, Katholieke Universiteit Leuven, 2004; 183–189.
27. Smirnov S, Lacor C, Baelmans M. A finite volume formulation for compact schemes with applications to LES. *Fifteenth AIAA CFD Conference*, AIAA paper, Anaheim, CA, U.S.A., 2001; 2001–2546.
28. Lacor C, Smirnov S, Baelmans M. A finite volume formulation of compact central schemes on arbitrary structured grids. *Journal of Computational Physics* 2004; **198**(2):535–566.
29. Winckelmans GS, Wray AA, Vasilyev OV. Testing of a new mixed model for LES: the Leonard model supplemented by a dynamic Smagorinsky term. *Proceedings of the Summer Program*, Center for Turbulence Research, Stanford, U.S.A., 1998; 367–388.
30. Germano M, Piomelli U, Moin P, Cabot WH. A dynamic subgrid-scale eddy viscosity model. *Physics of Fluids A* 1991; **3**:1760–1765.
31. Pope SB. Ten questions concerning the large-eddy simulation of turbulent. *New Journal of Physics* 2004; **6**:35.
32. Meyers J, Geurts BJ, Baelmans M. Optimality of the dynamic procedure for large-eddy simulations. *Physics of Fluids* 2005; **17**:045108.
33. Meyers J, Sagaut P, Geurts BJ. Optimal model parameters for multi-objective large-eddy simulations. *Physics of Fluids* 2006; **18**:095103.
34. Comte-Bellot G, Corrsin S. Simple Eulerian time correlation of full- and narrow-band velocity signals in grid-generated, 'isotropic' turbulence. *Journal of Fluid Mechanics* 1971; **48**(2):273–337.
35. Shukla RK, Zhong XL. Derivation of high-order compact finite difference schemes for non-uniform grid using polynomial interpolation. *Journal of Computational Physics* 2005; **204**(2):404–429.

DOI: 10.1002/fld